PHYSICAL REVIEW D **71,** 021303(R) (2005)

Cosmological lower bound on dark matter masses from the soft gamma-ray background

Kyungjin Ahn and Eiichiro Komatsu

Department of Astronomy, University of Texas at Austin, 1 University Station, C1400, Austin, Texas 78712, USA

(Received 22 October 2004; published 7 January 2005)

Motivated by a recent detection of 511 keV photons from the center of our Galaxy, we calculate the spectrum of the soft γ-ray background of the redshifted 511 keV photons from cosmological halos. Annihilation of dark matter particles into electron-positron pairs makes a substantial contribution to the γ-ray background. Mass of such dark matter particles must be $\lesssim 100$ MeV so that resulting electron-positron pairs are nonrelativistic. On the other hand, we show that in order for the annihilation not to exceed the observed background, the dark matter mass needs to be $\gtrsim 20$ MeV. We include the contribution from the active galactic nuclei and supernovae. The halo substructures may increase the lower bound to $\gtrsim 60$ MeV.

DOI: 10.1103/PhysRevD.71.021303 PACS numbers: 95.35.+d, 95.85.Nv, 95.85.Pw

A narrow 511 keV γ-ray line from the central part of our Galaxy has been detected and mapped by the SPI spectrometer on the international gamma-ray astrophysics laboratory (INTEGRAL) satellite [1]. This line is produced by annihilation of nonrelativistic electron-positron pairs, and one of the possible origins is the dark matter particles annihilating into electron-positron pairs [2], which explains the measured injection rate of positrons and morphology of the signal extended over the bulge region. Therefore, 511 keV lines from our Galaxy as well as other galaxies may provide a smoking gun for the existence of light dark matter particles [3]. Motivated by this idea, we calculate the spectrum of possible hard x-ray/soft γ-ray background (at $h\nu \sim 10 - 511$ keV) from the dark matter annihilation within cosmological halos distributed over a large redshift range. [4,5] have considered similar calculations at much higher energy ($\gtrsim 1$ GeV), assuming that the signal is coming from annihilation of neutralinos whose mass is of order $30 - 1000$ GeV; thus, their calculations cannot be applied to the energy scale we consider in this paper. Also, we improve upon the previous calculations of this sort by explicitly including the free streaming and the Jean's mass scale of dark matter particles, which naturally (rather than arbitrarily) sets the lower bound to the mass of dark matter halos.

The soft γ-ray background has been measured by the A4 low energy detectors and the A4 medium energy detectors on the HEAO-1 (high energy astronomy observatories 1) satellite as well as a balloon experiment [6]. Therefore, by comparing our calculations to observations, one can constrain the properties of dark matter. As the line is narrow, the signal must come from nonrelativistic electron-positron pairs; thus, the mass of dark matter particles must satisfy 511 keV $\lesssim m_X \lesssim 100$ MeV [2]. We calculate the background intensity, I_ν, as [7]

$$I_\nu = \frac{c}{4\pi}\int \frac{dz P_\nu([1+z]\nu, z)}{H(z)(1+z)^4}, \tag{1}$$

where ν is an observed frequency, $H(z)$ is the expansion rate at redshift z, and $P_\nu(\nu, z)$ is the (proper) volume emissivity of 511 keV photons:

$$P_\nu = \delta[(1+z)\nu - \nu_{511}]\alpha_{511} h\nu_{511}\langle\sigma v\rangle n_X^2. \tag{2}$$

Note that an electron-positron pair creates two 511 keV photons, and we assume that the universe is optically thin at $h\nu \gtrsim 10$ keV. α_{511} is the fraction producing an electron-positron pair per one dark matter annihilation process. If annihilation occurs predominantly via positronium formation, then $\alpha_{511} = 1/4$. While the positronium formation may be the dominant process in our Galaxy [8], we assume that annihilation occurs directly, $\alpha_{511} = 1$, for other galaxies. Here, $h\nu_{511} = 511$ keV and $\langle\sigma v\rangle$ is the thermally averaged annihilation cross section. For $\Omega_X h^2 = 0.116$ [9] one finds $\langle\sigma v\rangle = [3.4, 2.4, 2.9]10^{-26}\,\mathrm{cm^3\,s^{-1}}$ (or [1.1, 0.80, 0.97] pb) for $m_X = [1, 10, 100]$ MeV, respectively, (e.g., Eq. (1) in [10]). Here, we assume that $\langle\sigma v\rangle$ is velocity-indepedent (S-wave annihilation). Boehm *et al.* [2] argue that the S-wave cross section overpredicts the flux from the Galactic center; however, we argue that it is still consistent with the data for $m_X \gtrsim 20$ MeV and $\rho \propto r^{-0.4}$ (or shallower). This profile explains morphology of the Galactic signal [2], and one then finds that $\langle\sigma v\rangle \sim 0.8\mathrm{pb}(m_X/20\ \mathrm{MeV})^2$ is allowed at the 2-σ level (see Eq. (9) in [3] where the right-hand side should be multiplied by $37.6/17.3 \simeq 2.2$ for $\rho \propto r^{-0.4}$). As we show later, constraints from γ-ray background favor this parameter range, and our results do not violate the Galactic constraint.

Using the mass density $\rho_X \equiv n_x m_X$ and multiplying Eq. (1) by $\nu = \nu_{511}/(1+z)$, one obtains

$$\begin{aligned}\nu I_\nu &= \frac{c}{H(z)(1+z)^4}\cdot\frac{h\nu_{511}\langle\sigma v\rangle}{4\pi m_X^2}\langle\rho_X^2\rangle_z \\ &\simeq 0.4179\,\mathrm{keV\,cm^{-2}\,s^{-1}\,str^{-1}}\times\frac{C_X(z)(1+z)^2(\Omega_X h^2)^2}{\sqrt{\Omega_m h^2(1+z)^3+\Omega_\Lambda h^2}} \\ &\quad\times\left(\frac{\langle\sigma v\rangle}{10^{-26}\mathrm{cm^3\,s^{-1}}}\right)\left(\frac{1\,\mathrm{MeV}}{m_X}\right)^2,\end{aligned} \tag{3}$$

where $1 + z = \nu_{511}/\nu$, $\langle\rho_X^2\rangle_z$ is ρ_X^2 averaged over proper

volume at z, and $C_X(z) \equiv \langle \rho_X^2 \rangle_z / \langle \rho_X \rangle_z^2$ is the dark matter clumping factor. [We have used $\langle \rho_X \rangle_z = 10.54 \Omega_X h^2 (1+z)^3$ keV cm^{-3}.] It is worth noting that since $\langle \sigma v \rangle \propto (\Omega_X h^2)^{-1}$ [11], the intensity scales approximately as $\nu I_\nu \propto [C_X(z)/m_X^2](\Omega_X/\Omega_m^{1/2}) h (1+z)^{1/2}$ for $z > 1$; thus, the larger the particle mass is, the smaller the predicted γ-ray background becomes ($\propto m_X^{-2}$), and cosmology and redshift (or ν) dependence of the signal is almost entirely determined by $C_X(z)$, i.e., how dark matter clumpiness evolves with redshift. Throughout this paper, we adopt the best-fit power-law ΛCDM model from the first year Wilkinson Microwave Anisotropy Probe (WMAP) satellite [9].

Equation (3) allows one to calculate the intensity directly from N-body simulations which, in principle, give the full evolution of $C_X(z)$; however, such simulations are computationally challenging as they must resolve individual halo profiles at small distances (e.g., $\sim$kpc) in a large simulation box (e.g., $\sim$1 Gpc), which requires a large number of particles. Instead, we take an alternative approach. The clumping factor is essentially determined by the clumping of individual halos and the volume occupied by halos (or the number of halos). The former can be obtained by simulating individual halos using high-resolution simulations with smaller box sizes, while the latter can be obtained by simulating many halos using low-resolution simulations with larger box sizes. Therefore, by combining these simulations, one can calculate the clumping factor. This somewhat empirical approach, called a halo approach (see [12] for a review), turns out to be very powerful in making accurate predictions for clustering of dark matter particles in a highly nonlinear regime. By using this approach, we calculate $C_X(z)$ as

$$C_X(z) = \frac{(1+z)^3}{\langle \rho_X \rangle_z^2} \int_{M_{\rm min}}^{\infty} dM \frac{dn(M,z)}{dM} \int d^3 r \rho_X^2(M,r), \quad (4)$$

where $\rho_X(M,r)$ is a dark matter halo profile, and $dn(M,z)/dM$ is the comoving number density of halos in the mass range of $M \sim M + dM$ at z. For dn/dM we adopt an empirical fit to N-body simulations obtained by [13] with $a = 0.75$, $p = 0.3$, and $A = 0.322$ (see [13] for the detail). Why does the integral in Eq. (4) have a minimum mass? When the length scale is smaller than the free-streaming scale and/or Jean's scale of the dark matter particles, density fluctuations are suppressed and halos do not form. Although the actual effect is not an abrupt cutoff at these mass scales, we approximate it as the low mass cutoff in the integral; thus, no halo would form below $M_{\rm min} = \max(M_F, M_J)$, where M_F is the free-streaming mass and M_J is the dark matter Jean's mass. For M_F, we adopt the expression obtained by [14]: $M_F \approx (4\pi/3)\overline{\rho}_m (\lambda_F/2)^3$, where $\lambda_F \equiv 2.72 (\Omega_X h^2)^{1/3} \times (m_X/1\ {\rm keV})^{-4/3}$ Mpc, and $\overline{\rho}_m$ is the presentday mean matter density. With this definition one obtains [14]

$$M_F = 8.3 \cdot 10^{-2} M_\odot \left(\frac{\Omega_m h^2}{0.13}\right)\left(\frac{\Omega_X h^2}{0.11}\right)\left(\frac{m_X}{1\ {\rm MeV}}\right)^{-4}. \quad (5)$$

The dark matter Jean's mass is given by [15]

$$M_J = 38.79 M_\odot \left(\frac{m_X}{\rm MeV}\right)^{-3}\left(\frac{x_F}{12}\right)^{3/2}\left(\frac{1+z}{3069}\right)^{3/2}, \quad (6)$$

for $1 + z > 1 + z_{eq} \simeq 3069$, which is a valid expression for cold thermal relics which decouple from radiation at $x_F = m_X/T_F > 3$ ($x_F \approx [11-15]$ for $m_X \approx [1-100]$ MeV;, e.g., see [10]).

Equation (4) can be cast into the product of the collapse fraction and the mean "halo clumping factor":

$$C_X(z) = \Delta \cdot F_{\rm coll}(z) \cdot [C_X^{\rm halo}], \quad (7)$$

where Δ is the mean halo overdensity of a halo in units of the cosmic mean matter density, the collapse fraction $F_{\rm coll}(z) \equiv \int dM \frac{dn}{dM} M/\overline{\rho}_m$ is the mass fraction collapsed into cosmological halos at z, $[A] \equiv \int dM \frac{dn}{dM} MA / \int dM \frac{dn}{dM} M$, and $C_X^{\rm halo} \equiv \int d^3 r (\frac{\rho_X}{\langle \rho_X \rangle_{\rm halo}})^2 / \int d^3 r$ is the "halo clumping factor" defined in terms of the halo mean density $\langle \rho_X \rangle_{\rm halo} \equiv \int d^3 r \rho_X / \int d^3 r = \Delta \cdot \langle \rho_X \rangle_z$. As illustrated in Fig. 2, the early time $C_X(z)$ is mainly determined by $F_{\rm coll}(z)$, while the late time $C_X(z)$ by $[C_X^{\rm halo}]$. As it can be seen from Eq. (4), $C_X(z)$ is very sensitive to the density profile, whose properties are not fully understood (or observed) yet. In order to quantify uncertainties associated with the density profile, therefore, we adopt two different models for density profiles.

Case A: The Navarro-Frenk-White (NFW) Profile—The NFW profile is an empirical fit to radial profiles of dark matter halos in N-body simulations [16]. This profile has a central cusp, $\rho_X \propto r^{-1}$, and is therefore expected to produce large annihilation signals. The NFW profile is given by $\rho_X(r) = \rho_s (r/r_s)^{-1}(1 + r/r_s)^{-2}$ [16]. The mass M enclosed within the virial radius, $r_{\rm vir}$, is $M = 4\pi \rho_s r_s^3 [\ln(1+c) - c/(1+c)]$, and the scale radius, r_s, is $r_s = r_{\rm vir}/c$, where c is called the concentration parameter. With these definitions, one obtains

$$C_X^{\rm halo} = \frac{c^3 [1 - 1/(1+c)^3]}{9[\ln(1+c) - c/(1+c)]^2}. \quad (8)$$

For instance, $C_X^{\rm halo}(c=3) = 7.3$, $C_X^{\rm halo}(c=10) = 50$, $C_X^{\rm halo}(c=20) = 203$. For Δ, we use an approximate form $\Delta = (18\pi^2 + 82x - 39x^2)/\Omega(z)$, where $\Omega(z)$ is the ratio of mean matter density to the critical density at z, and $x = \Omega(z) - 1$. This expression is valid for a flat ΛCDM universe [17,18]. The concentration of dark matter halos found in N-body simulations has a log-normal distribution with a median value of [18]

$$c(M,z) = 4 \frac{1+z_c}{1+z}, \quad (9)$$

where the collapse redshift, z_c, is implicitly given by a relation $M_*(z_c) = 10^{-2} M$. ($M_*(z)$ is the nonlinear mass at

z.) As lower mass objects collapse at higher z_c, the concentration decreases as M. Following [19], we take into account a log-normal distribution of c with the dispersion of $\sigma[\ln(c)] = 0.2$. While we use Eq. (9) for all the range of M and z in our analysis, we should keep in mind that this fitting formula is valid only for a limited range of M and z covered by N-body simulations.

Figure 1 shows the predicted soft γ-ray background for the NFW profile. The predicted signal, νI_ν, is roughly proportional to $\nu^{1.3}$, which simply reflects the fact that the universe becomes more clumpy at lower z as $C(z) \propto (1+z)^{-1.8}$ (recall that $h\nu = 511\ \mathrm{keV}/(1+z)$), as seen in Fig. 2. One should, however, keep in mind that we have simply extrapolated the fitting formula for $c(M, z)$ [Eq. (9)] to the regime where simulations are no longer valid. For the $m_X = 1$ MeV case, for example, the free-streaming mass gives the maximum concentration of $c \sim 70$ at $z = 0$. Since we do not fully understand halo profiles at such low mass or high concentration, we also apply an arbitrary, hypothetical upper limit to c and investigate sensitivity of our results to the change in concentration parameters. This toy model will substantially reduce the contribution from small mass halos with $c(M, z) > c_{\max}$. As $c(M, z) \propto (1+z)^{-1}$, the signal at lower z (higher $h\nu$) is suppressed. As a result, νI_ν becomes almost flat for $\nu > \nu_*$, where ν_* corresponds to a redshift, z_*, after which the clumping factor stops evolving fast and evolves only slowly as $(1+z)^{-1/2}$ or even slower (Fig. 1 and 2). Sensitivity of the predicted spectrum to the concentration parameter model is demonstrated more in Fig. 3. For the canonical concentration parameter model given by Eq. (9) without any upper limit, the smallest mass halos always dominate; on the other hand, once the upper limit on c is imposed, the largest contribution comes from $M \simeq M_*(z)$, effectively removing contribution from the lower mass halos as the lower mass halos hit $c_{\max}$ earlier than the higher mass halos.

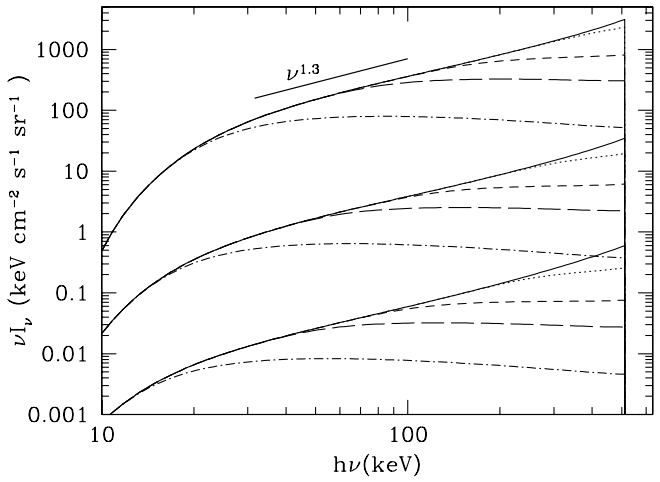

FIG. 1. Predicted spectrum of the soft γ-ray background from cosmological halos with the NFW profile. From the top to the bottom, each set of curves represent $m_X = 1, 10, 100$ MeV. The solid lines show the canonical concentration model [Eq. (9)], while the dotted, short-dashed, long-dashed, and dashed-dotted curves show the models with upper cutoffs of $c_{\max} = 50, 20, 10$, and 3, respectively. Signals without upper cutoffs are well fit by a power law for $\nu \gtrsim 40$ keV, as indicated by the uppermost line.

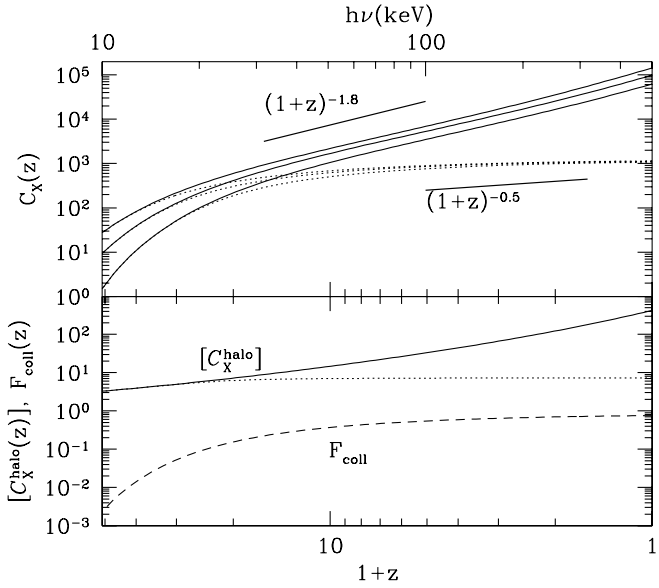

FIG. 2. Upper panel: The clumping factor $C_X(z)$ for different m_X's. Solid lines, from the bottom to the top, represent the clumping factor for $m_X = [1, 10, 100]$ MeV respectively. Dotted lines represent the clumping factor for $c_{\max} = 3$, also with the same meaning from the bottom to the top. Two power laws reflecting the asymptotic behavior of $C_X(z)$ are also plotted. The trend for different mass curves indicates the fact that the minimum halo mass is smaller for larger m_X, thus obtaining higher clumping. Lower panel: The mean halo clumping factor $[C_X^{\mathrm{halo}}(z)]$ and the collapse fraction $F_{\mathrm{coll}}(z)$ for $m_X = 1$ MeV. The solid line is for no upper limit on c, while the dotted line is for $c_{\max} = 3$. It clearly shows that the low redshift behavior is determined mainly by $[C_X^{\mathrm{halo}}(z)]$, while the high redshift behavior by $F_{\mathrm{coll}}(z)$.

Case B: The Truncated Isothermal Sphere (TIS) Profile—The TIS [20] is an analytical model of the post collapse equilibrium structure of halos resulting from the collapse of a top-hat density perturbation. The TIS is the minimum energy solution to the Lane-Emden equation, matching energy of the TIS to the energy of the top-hat perturbation. The TIS density profile has a soft core and thus provides a much smaller annihilation signal than the NFW profile. Note that the TIS fits the observed rotation curves of dwarf spheroidals and low surface brightness galaxies fairly well, as opposed to the NFW. The TIS density profile is given by [20]

$$\rho = 1799\overline{\rho}_m(z)\left[\frac{21.38}{9.08^2 + (r/r_0)^2} - \frac{19.81}{14.62^2 + (r/r_0)^2}\right], \quad (10)$$

for $r < r_t$. Here, $\overline{\rho}_m(z)$ is the mean matter density at z, r_t is the truncation radius,

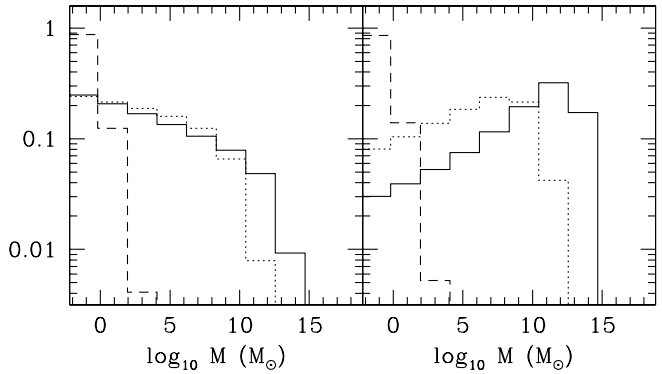

FIG. 3. Fractional contribution from different NFW halo masses at different redshifts. The left panel shows the canonical concentration model [Eq. (9)] with no upper limit, while the right panel shows the model with $c_{\max} = 3$. In both panels, the solid, dotted, and dashed lines correspond to $z = 0$, 4, and 50, respectively.

$$r_t = \frac{0.187}{1+z}\left(\frac{M}{10^{12}M_\odot}\right)(\Omega_m h^2)^{-1/3}\ \text{Mpc}, \qquad (11)$$

and r_0 is the core radius given by $r_0 = r_t/29.4$. We find that the predicted signal for the TIS model is very similar to that for the NFW with $c_{\max} = 3$, which is consistent with the TIS profile being much flatter (i.e., much less clumpy) than the NFW with the canonical concentration. This can be more easily explained by Eq. (7). At $z \gtrsim 1$, $\Delta \approx 178$ and $C_X(z) \approx 178 \times 7.3 \times F_{\rm coll}$ for the NFW with $c_{\max} = 3$, while the TIS has $\Delta \approx 130$, $C^{\rm halo} \approx 11.5$, and so $C_X(z) \approx 130 \times 11.5 \times F_{\rm coll}$.

AGNs and Supernovae—There are other sources for the soft γ-ray background. The Active Galactic Nuclei (AGNs) are probably the most dominant contribution up to $\sim$100 keV, and it may continue to dominate up to $\sim$500 keV [21,22], depending on a cutoff energy scale of the AGN spectrum, $E_{\rm cut}$, which is a free parameter. The other candidate source is the Type Ia Supernovae (SNIa). [23] have calculated a spectrum of the soft γ-ray background from SNIa, finding that the SNIa contribution can account for the observed intensity. Our recent calculations, however, show that they overestimated the signal by a factor of $\sim$10 (they assumed $\sim$10 times larger supernova rate than observed). The SNIa contribution is thus negligible at the energy scale of our interest [24]. Figure 4 compares the dark matter annihilation, the Compton-thin AGNs with $E_{\rm cut} = 500$ keV [22], and the supernovae contribution [24], as well as the observed soft γ-ray background [6]. We find that an acceptable range for the dark matter mass is $20 \lesssim m_X \lesssim 100$ MeV for the NFW profile. (Note that the upper limit comes from requiring that electron-positron pairs be nonrelativistic.) The uncertainty includes statistical uncertainty as well as potential systematic uncertainties associated with instrumental calibrations. Background signals measured by various experiments show a large scatter (e.g., [25]), and it may be possible that the measured background is uncertain up to 30% [22].

One may relax this constraint in various ways. If the AGN spectrum has a smaller energy cutoff, $E_{\rm cut} \sim 100$ keV, the AGNs do not contribute to the γ-ray background for $h\nu \gtrsim 100$ keV, and $m_X \gtrsim 12$ MeV becomes acceptable (Fig. 5). Bigger uncertainties come from the halo model. If we adopt the TIS or the NFW with $c_{\max} = 3$, we obtain $m_X \gtrsim 5$ and 1.7 MeV for with and without the AGNs contribution, respectively, (see Fig. 4 and 5). Such a low concentration parameter or filtering of low mass halos may be possible if dark matter has some finite self-interacting cross section [26,27]. In addition to the average shape of ρ_X, the clumpy substructure within halos would contribute to the signal significantly [4,19]. While their abundance and properties are uncertain, the analysis in [4] shows that substructures can enhance the clumping factor by more than a factor of 10. As the intensity is proportional to m_X^{-2}, the contribution from substructures can increase the lower limit on m_X by more than a factor of 3, giving $m_X \gtrsim 60$ MeV for the NFW profile.

In summary, we have calculated the soft γ-ray background of the redshifted 511 keV photons from the dark matter particles annihilating into electron-positron pairs in cosmological halos. Our fiducial model based on the current N-body simulations, compared to the observed γ-ray spectrum, places limits on the dark matter mass, $20 \lesssim m_X \lesssim 100$ MeV. (If the cross section is allowed to be free, we find $(\langle\sigma v\rangle/\text{pb})(\text{MeV}/m_X)^2 \lesssim 2.1 \times 10^{-3}$, which is consistent with that from the Galactic center [3] for $\rho \propto r^{-0.4}$ or shallower profile). Recently, Beacom,

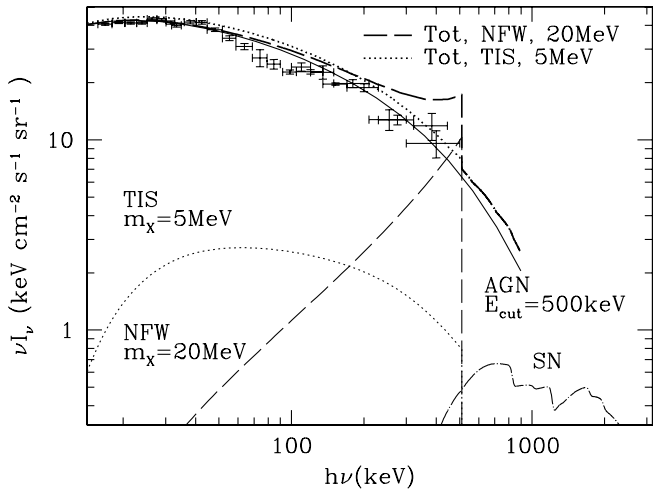

FIG. 4. Comparison of the dark matter annihilation (dashed lines for the NFW and dotted lines for the TIS), the Compton-thin AGNs [22] (solid), and the type Ia supernovae contribution (dashed-dotted), as well as the observed soft γ-ray background [6] (points with errors). The predicted total signals are plotted as the thick dashed and dotted lines, which set upper limits on the dark matter mass from the measured points.

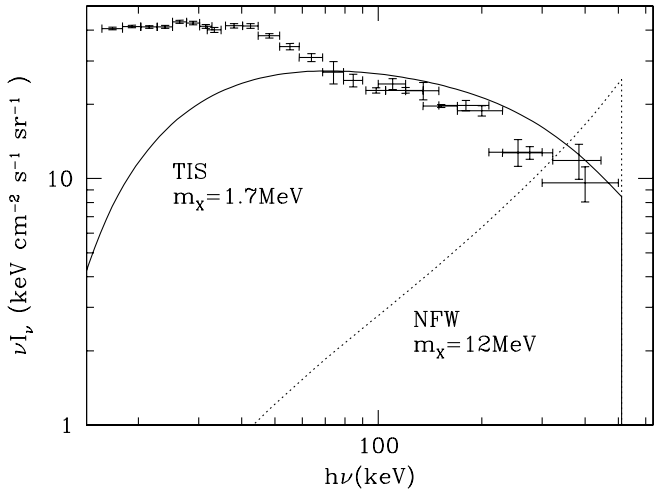

FIG. 5. Dark matter annihilation only. Smaller dark matter masses are allowed. (see also Fig. 4.)

Bell, and Bertone [28] have shown that the internal bremsstrahlung of electrons and positrons contributes to the γ-ray background at >1 MeV. Using COMPTEL and EGRET data, they have obtained $m_X \lesssim 20$ MeV. Putting all the constraints together, $m_X \sim 20$ MeV may be favored. However, in order to have a more robust constraint, further understanding of cosmological nonlinear structures is required. Obtaining a more reliable model for AGNs is equally important. Uncertainty in the cutoff energy, $E_{\rm cut}$, is the dominant uncertainty in the predicted soft γ-ray background signal at $h\nu \gtrsim 100$ keV. If the cutoff energy is smaller than $\sim$100 keV, the soft γ-ray background signal may serve as evidence for the existence of dark matter particles with $m_X \sim \mathcal{O}(10)$ MeV.

We would like to thank D. E. Gruber for providing us with the HEAO-1 data, and Y. Ueda for providing us with the AGN predictions. We would like to thank E. R. Fernandez for bringing our attention to this subject, and G. Bertone, D. E. Gruber, R. E. Rothschild, and P. R. Shapiro for valuable discussion. K. A. was partially supported by NASA Astrophysical Theory Program Grant Nos. NAG5-10825, NAG5-10826, NNG04G177G, and Texas Advanced Research Program Grant No. 3658-0624-1999.

[1] P. Jean *et al.*, Astron. Astrophys. **407**, L55 (2003); J. Knödlseder *et al.*, Astron. Astrophys. **411**, L457 (2003).
[2] C. Boehm, D. Hooper, J. Silk, M. Casse, and J. Paul, Phys. Rev. Lett. **92**, 101301 (2004).
[3] D. Hooper, F. Ferrer, C. Boehm, J. Silk, J. Paul, N. W. Evans, and M. Casse, Phys. Rev. Lett., **93**, 161302 (2004).
[4] J. Taylor and J. Silk, Mon. Not. R. Astron. Soc. **339**, 505 (2003).
[5] D. Elsäesser and K. Mannheim, Astropart. Phys. **22**, 65 (2004).
[6] D. E. Gruber, J. L. Matteson, L. E. Peterson, and G. V. Jung, Astrophys. J. **520**, 124 (1999); Y. Fukada, S. Hayakawa, I. Kasahara, F. Makino, Y. Tanaka, and B. V. Sreekantan, Nature (London) **254**, 398 (1975).
[7] J. A. Peacock, *Cosmological Physics* (Cambridge University Press, Cambridge, England, 1999), p. 91–94.
[8] R. L. Kinzer, P. A. Milne, J. D. Kurfess, M. S. Strickman, W. N. Johnson, and W. R. Purcell, Astrophys. J. **559**, 282 (2001).
[9] D. N. Spergel *et al.*, Astrophys. J. Suppl. Ser. **148**, 213 (2003).
[10] C. Boehm, T. A. Ensslin, and J. Silk, J. Phys. G **30**, 279 (2004).
[11] E. W. Kolb and M. S. Turner, *The Early Universe* (Addison-Wesley, Reading, MA, 1990), Eq. (5.47).
[12] A. Cooray and R. Sheth, Phys. Rep. **372**, 1 (2002).
[13] R. K. Sheth and G. Tormen, Mon. Not. R. Astron. Soc. **329**, 61 (2002).
[14] J. Sommer-Larsen and A. Dolgov, Astrophys. J. **551**, 608 (2001); V. Avila-Reese, P. Colín, O. Valenzuela, E. D'Onghia, and C. Firmani, Astrophys. J. **559**, 516 (2001).
[15] P. Coles and F. Lucchin, *Cosmology* (John Wiley & Sons, New York, 1995), Eq. (13.5.10).
[16] J. F. Navarro, C. S. Frenk, and S. D. White, Astrophys. J. **490**, 493 (1997).
[17] G. L. Bryan and M. L. Norman, Astrophys. J. **495**, 80 (1998).
[18] J. S. Bullock, T. S. Kolatt, Y. Sigad, R. S. Somerville, A. V. Kravtsov, A. A. Klypin, J. R. Primack, and A. Dekel, Mon. Not. R. Astron. Soc. **321**, 559 (2001).
[19] P. Ullio, L. Bergström, J. Edsjö, and C. Lacey, Phys. Rev. D **66**, 123502 (2002).
[20] P. R. Shapiro, I. T. Iliev, and A. C. Raga, Mon. Not. R. Astron. Soc. **307**, 203 (1999); I. T. Iliev and P. R. Shapiro, Mon. Not. R. Astron. Soc. **325**, 468 (2001).
[21] A. Comastri, G. Setti, G. Zamorani, and G. Hasinger, Astron. Astrophys. **296**, 1 (1995).
[22] Y. Ueda, M. Akiyama, K. Ohta, and T. Miyaji, Astrophys. J. **598**, 886 (2003).
[23] L.-S. The, M. D. Leising, and D. D. Clayton, Astrophys. J. **403**, 32 (1993).
[24] K. Ahn *et al.* (to be published).
[25] M. Revnivtsev, M. Gilfanov, R. Sunyaev, K. Jahoda, and C. Markwardt, Astron. Astrophys., **411**, 329 (2003).
[26] D. N. Spergel and P. J. Steinhardt, Phys. Rev. Lett. **84**, 3760 (2000).
[27] K. Ahn and P. R. Shapiro, astro-ph/0412169.
[28] J. F. Beacom, N. F. Bell, and G. Bertone, astro-ph/0409403.